A New Approach to the Electrochemical Metallization of Organic Monolayers: Palladium Deposition onto a 4,4′-Dithiodipyridine Self-Assembled Monolayer

ARTICLE *in* ADVANCED MATERIALS · DECEMBER 2004

Impact Factor: 17.49 · DOI: 10.1002/adma.200400409

7 AUTHORS, INCLUDING:

Valentina Ivanova

Atomic Energy and Alternative Energies Co…

49 PUBLICATIONS **770** CITATIONS

SEE PROFILE

ADVANCED MATERIALS

from the matrix to the reinforcements through the interface during loading. Second, the matrix surrounding the reinforcement particles is reinforced by carbon nanotubes. Third, carbon nanotubes may promote formation of microcracks in the interface, inhibiting larger crack growth along the interface (as shown in Fig. 5b); these microcracks may also explain the increase in toughness and strain to fracture.

In conclusion, we have shown that aligned carbon nanotubes can be grown on micrometer–sized SiC particles by CVD. SiC/carbon nanotube hybrid particles can have wide applications in many fields, such as particle reinforcement composites, field emission, etc. The application of this kind of SiC/carbon nanotube hybrid filler in an epoxy composite provided an evident improvement in mechanical properties, which is ascribed to a new type of interfacial structure.

Experimental

Our experimental setup is an electrical furnace (40 cm long) equipped with a quartz tube (inner diameter 40 mm). Xylene was used as the carbon source, and ferrocene as the catalyst. First, as-received Norton SiC powder (two types of SiC powder were used, with particle sizes of 10–20 μm and 1–4 μm) was dispersed on a flat ceramic boat; the thickness of SiC particle layer was about 0.5 mm. This boat was then placed in the center of the quartz tube. After that, the furnace was heated to the growth temperature (650–850 °C). While heating the furnace, N_2 flowed through the reactor at a rate of 100 sccm. After the furnace reached the growth temperature, the buffer gas was changed to N_2/H_2 (in a 10:1 ratio) and the flow rate was increased to 1650 sccm. The feedstock mixture (with a ferrocene content of 0.02 g mL^{-1} in xylene) was added with an injector at a rate of about 0.1 mL min^{-1}. Generally, the growth time was ≈ 10–30 min. After the furnace was cooled to room temperature (under a N_2 flow, 100 sccm), the product was collected from the reactor.

For fabrication of composite, the SiC (average size 17 μm)/carbon nanotube particles (with a content of 0.5 wt.-%) were directly mixed into a liquid epoxy (Struers Epofix resin, bisphenol A-epichlorhydrin, and hardener, triethylenetetramine, in a 10.7 wt.-% proportion), and stirred with a mechanical mixer. The composite suspension was poured into a dog-bone silicone mold with a gauge length of 30 mm, a width of 6 mm, and a thickness of about 3 mm. The cure time for this composite was 4 days. Samples without filler and with nanotube-free SiC particles were also fabricated for comparison. Tensile tests were conducted on an Instron materials testing machine at a loading rate of 0.5 mm min^{-1} with an extensometer of gauge length 12.5 mm ± 2.5 mm.

The transmission electron microscopy (TEM) and scanning electron microscopy (SEM) observations were performed using a Jeol 1200 TEM operating at 120 kV and a Leo 1530 FEG SEM, respectively.

Received: March 12, 2004
Final version: June 28, 2004

[1] S. Iijima, *Nature* **1991**, *354*, 56.
[2] a) *Carbon Nanotubes: Synthesis, Structure, Properties and Applications* (Eds: M. S. Dresselhaus, G. Dresselhaus, P. Avouris), Springer, New York **2001**. b) E. T. Thostenson, Z. F. Ren, T. W. Chou, *Compos. Sci. Technol.* **2001**, *61*, 1899.
[3] E. T. Thostenson, W. Z. Li, D. Z. Wang, Z. F. Ren, T. W. Chou, *J. Appl. Phys.* **2002**, *91*, 6034.
[4] R. Andrews, D. Jacques, A. M. Rao, F. Derbyshire, D. Qian, X. Fan, E. C. Dickey, J. Chen, *Chem. Phys. Lett.* **1999**, *303*, 467.
[5] B. Q. Wei, R. Vajtai, Y. Jung, J. Ward, R. Zhang, G. Ramanath, P. M. Ajayan, *Nature* **2002**, *416*, 495.
[6] A. Cao, R. Baskaran, M. J. Frederick, K. Turner, P. M. Ajayan, G. Ramanath, *Adv. Mater.* **2003**, *15*, 1105.
[7] A. Cao, G. Meng, P. M. Ajayan, *Adv. Mater.* **2004**, *16*, 40.
[8] M. Kusunoki, T. Suzuki, C. Honjo, T. Hirayama, N. Shibata, *Chem. Phys. Lett.* **2002**, *366*, 458.
[9] A. Cao, P. M. Ajayan, G. Ramanath, *Appl. Phys. Lett.* **2004**, *84*, 109.
[10] Y. J. Jung, B. Wei, R. Vajtai, P. M. Ajayan, Y. Homma, K. Prabhakaran, T. Ogino, *Int. Chem. Eng.* **2003**, *3*, 561.
[11] N. Koratkar, B. Wei, P. M. Ajayan, *Adv. Mater.* **2002**, *14*, 997.
[12] E. Carreño-morelle, S. E. Urreta, R. Schaller, *Acta Mater.* **2000**, *48*, 4725.

A New Approach to the Electrochemical Metallization of Organic Monolayers: Palladium Deposition onto a 4,4′-Dithiodipyridine Self-Assembled Monolayer**

By *Thorsten Baunach*, *Valentina Ivanova*, *Dieter M. Kolb*,* *Hans-Gerd Boyen*, *Paul Ziemann*, *Michael Büttner*, and *Peter Oelhafen*

The use of single molecules as nanoelectronic devices has received continuing interest in recent years. One of the main problems is the electrical contact between molecules and the outside world.[1] To establish permanent contacts, several sophisticated techniques have been reported.[2–4] One possibility is to deposit gold nanoparticles *on top* of a self-assembled monolayer (SAM),[5–7] and to contact these clusters with a scanning tunneling microscope (STM) tip[8] or a conducting cantilever of an atomic force microscope (AFM).[1]

To date, the deposition of a metal layer on top of a SAM, either from the gas phase[9,10] or electrochemically,[11–20] has not been successful. Failures are most often due to the fact that the deposited metal creeps underneath the SAM and becomes sandwiched between the gold substrate and the SAM. The classic route to the metallization of a non-conductive surface is currentless deposition, whereby metal ions are reduced using an appropriate redox system in solution and deposited onto a surface which provides the necessary nucleation cen-

[*] Prof. D. M. Kolb, Dr. T. Baunach, Dr. V. Ivanova
Abteilung Elektrochemie, Universität Ulm
D-89069 Ulm (Germany)
E-mail: dieter.kolb@chemie.uni-ulm.de
Dr. H.-G. Boyen, Prof. P. Ziemann
Abteilung Festkörperphysik, Universität Ulm
D-89069 Ulm (Germany)
Dr. M. Büttner, Dr. P. Oelhafen
Institut für Physik, Universität Basel
Klingelbergstr. 82, CH-4056 Basel (Switzerland)

[**] Financial support by the Deutsche Forschungsgemeinschaft (DFG) within SFB 569, the Swiss National Science Foundation (NF), and the Swiss National Center of Competence in Research (NCCR) "Nanoscale Science" is gratefully acknowledged.

  DOI: 10.1002/adma.200400409

ters (e.g., silver or gold plating on glass).[21] This method has also been applied to metal deposition onto aminothiol SAMs on gold.[22] However, convincing proof that the metal resides on top of the SAM is still lacking.

A crucial step towards ensuring that the deposit remains on top of a SAM is the proper ω-functionalization of the thiol, such as by nitrogen-containing end groups which are known to interact strongly with metal ions like Pd^{II} or Cr^{VI}.[23,24] An inherent disadvantage of currentless deposition, in principle a simple procedure, is the absence of any potential control. The start, growth rate, and termination of the deposition process are not as easily and precisely controlled as in the case of an electrochemical deposition. In the following, we describe a new approach to metal deposition on top of a functionalized SAM that combines elements of currentless and electrochemical deposition methods. Angle-resolved X-ray photoelectron spectroscopy (XPS) was used to prove that the palladium-metal deposit indeed resides on top of the SAM rather than underneath, as is usually observed in the case of electrochemical deposition from solution.

Figure 1 shows cyclic current–potential curves of the Pd^{II}-loaded, 4,4′-dithiodipyridine (PySSPy)-covered Au(111) electrode in 0.1 M H_2SO_4. In the first cycle (solid line), in the negative scan direction, a cathodic current peak (A) was found at

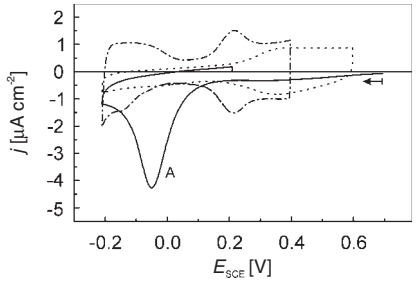

Figure 1. Cyclic current–potential curves of a PySSPy-modified Au(111) electrode in 0.1 M H_2SO_4. The first (solid line, starting at +0.7 V) and second (dotted line) cycles are shown. Before the experiment, the PySSPy-modified Au(111) sample was immersed in 0.1 mM $PdSO_4$ + 0.1 M H_2SO_4 for 15 min, to yield 0.3 ML of adsorbed Pd^{II}. For comparison, a Au(111) surface covered by 0.3 ML palladium without thiol is also shown (dashed–dotted line). Scan rate: 5 mV/s.

–0.05 V. The corresponding charge is 102 ± 10 μC cm^{-2}. In the second cycle (dotted line), this maximum is completely absent, indicating that an irreversible process has taken place at the surface. On a neat (palladium-ion free) PySSPy-Au(111) surface, no current peak was found in the corresponding potential range.[25] Thus, peak A can be assigned to the reduction of adsorbed Pd^{II} to Pd^0. In order to prove that Pd^{II} adsorbs selectively on the pyridinium end group, the electrode was modified with diphenyl disulfide (a substance similar to PySSPy, but without a reactive end group). After immersing this modified electrode into a Pd^{II} solution, no cathodic current peak was observed in the corresponding potential range. This clearly indicates that Pd^{II} specifically adsorbs on the pyridine moiety of the SAM. It should be mentioned that, for long incubation times (≈16 h), an additional cathodic maximum was found at about 0.4 V for both SAMs (PySSPy and diphenyl disulfide). This, however, is due to the reduction of Pd^{II}, which is chemisorbed directly on the gold surface. Thus, Pd^{II} can slowly penetrate the SAM.

How does the interaction between Pd^{II} and the pyridine species take place? There are two possibilities: an electrostatic interaction or complexation. The interaction between Pd^{II} (from a chloride-containing electrolyte) and a pyridine end group has been studied in neutral solution in detail by Dressick et al.[23] UV-vis absorption and XPS experiments indicated the formation of a $(Py)_2PdCl_2$ complex. Furthermore, the growth of large, chloro-bridged palladium oligomers was observed. To avoid the formation of oligomers, we used an acidic solution and avoided chloride. However, this has two consequences: protonation of the SAM, and the formation of sulfato complexes in solution. As previous studies have shown, the SAM is protonated at pH 1,[26–28] and thus the outer layer of the SAM is positively charged. Information about palladium–sulfato complexes is scarce.[29] Possible species in solution are Pd^{2+}, $PdSO_4$[30], and, only in small concentrations, $[Pd(SO_4)_2]^{2-}$.[31] Hence, an electrostatic interaction with the palladium ion is not very likely. Another possibility is that the uncharged palladium species forms a sulfato–amino complex $(Pd(SO_4)(Py)_2)$ with the SAM in which the palladium substitutes the hydrogen on top of the SAM. This complex is known from the solution phase.[32]

After having discussed possible forms of the adsorbed Pd^{II}, we will now focus on the reduced palladium. In particular, we will address the question of where the deposited metal is located: *underneath* or *on top of* the SAM. The cyclic current–potential curve obtained after Pd^{II} reduction (Fig. 1, dotted line) shows no characteristic peaks and differs markedly from the voltammogram for palladium-covered Au(111) electrodes, where peaks due to adsorption and absorption of hydrogen[33,34] are seen. It should be noted that, in our case, much less than a monolayer of palladium was deposited (i.e., about 0.25 ML). Therefore, a cyclic voltammogram for 0.3 ± 0.1 ML palladium deposited directly on a Au(111) electrode is shown for comparison (Fig. 1, dashed–dotted curve). Since the characteristic features of the latter are not observed for the dotted curve, we conclude that there are no uncovered palladium islands directly bound to the gold surface.

To investigate this in more detail, STM images were obtained. In Figure 2a, a representative image of the SAM-modified gold surface covered with Pd^0 islands is presented. Note that before recording this image, the electrode potential was kept at –0.1 V to reduce Pd^{II}. In contrast to a palladium-free PySSPy-surface,[25] no ordered thiol adlayer was observed, not even between the many islands. The islands are monoatomic in height[35] and cover about 30 % of the surface area. This corresponds quite well to the charge for the reduction of Pd^{II} mentioned above. Due to the small size of the islands, no atomic or molecular resolution could be obtained. This would have been useful for identifying the islands, either by measur-

ADVANCED MATERIALS

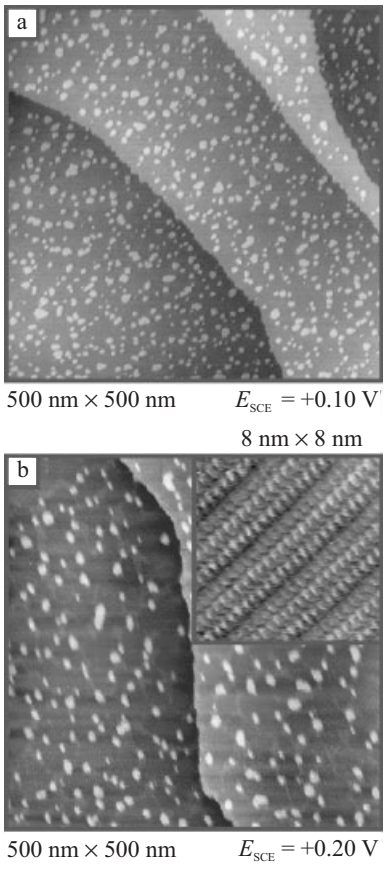

Figure 2. STM images of Au(111) electrodes in 0.1 M H_2SO_4. a) After modification with PySSPy and subsequent immersion for 1 min in 0.1 mM $PdSO_4$ + 0.1 M H_2SO_4. Monoatomic-high islands of the reduced Pd^0 are clearly seen. Before recording the image, the potential was set to –0.1 V to reduce adsorbed Pd^{II}. b) After depositing 0.3 ML palladium onto bare Au(111) and then immersing in PySSPy solution. The inset shows the ordered PySSPy-SAM on the Au(111). The islands represent palladium (see text).

ing the Pd–Pd distance or observing co-adsorbed sulfate. The islands were stable between –0.05 and 0.55 V, and did not change their shape. An interesting effect was observed if the same area was scanned several times with the STM tip. The number of islands was slightly reduced (not shown), as reported previously for palladium bound to an aminothiol-SAM.[22] In that case, Pd^{II} was reduced by an organic reductant. The movement of metal islands or clusters on the substrate with the STM tip not only reflects a relatively weak interaction between deposit and substrate, but also suggests that the deposit is on top of the SAM, rather than underneath. For further comparison, Figure 2b shows the surface of Au(111) onto which approximately 0.3 ML palladium was deposited before modifying the electrode for 5 min with PySSPy. Hence, in this case the palladium is underneath the SAM. Between the palladium islands, small ordered domains are seen (Fig. 2b, inset) which have the same structure as ordered thiol adlayers on bare Au(111).[25] Since such structures are not observed after reduction of Pd^{II} on SAM-modified surfaces, we conclude from the STM measurements that the palladium islands are on top of, rather than underneath, the organic layer.

In order to test this idea critically, angle-resolved XPS measurements were used to analyze the chemical state and, more importantly, the sequence of the individual layers by systematically varying the surface sensitivity (i.e., the probing depth) by correspondingly tuning the detection angle of the photoelectrons. In Figure 3, a series of high-resolution core-level spectra of the Au $4d_{3/2}$ and Pd $3d_{3/2}$ regions is shown, ac-

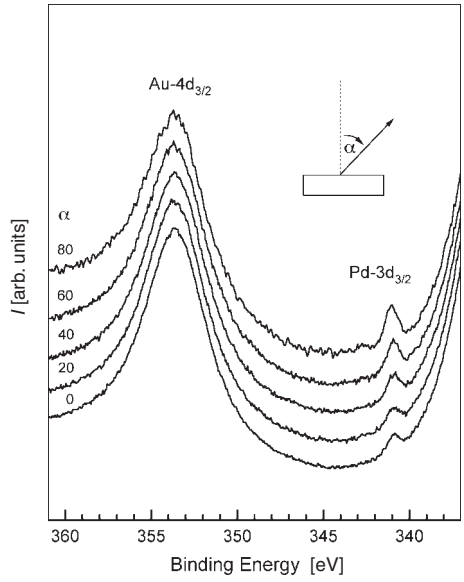

Figure 3. Angle-resolved Au $4d_{3/2}$ and Pd $3d_{3/2}$ core-level XP spectra acquired from a PySSPy-modified Au(111) sample after the electrochemical reduction of 0.3 ML of adsorbed Pd^{II} ions to Pd^0.

quired from a PySSPy-modified Au(111) sample after adsorption of 0.3 ML Pd^{II} by immersion into 0.1 mM $PdSO_4$ + 0.1 M H_2SO_4 for 15 min, followed by electrochemical reduction of Pd^{II} to Pd^0. The spectra were measured as a function of the photoelectron take-off angle α for angles between normal ($\alpha = 0°$) and grazing ($\alpha = 80°$) emission. For better comparison, all spectra have been normalized to give the same height of the gold signal.

Focusing first on the lowest curve, corresponding to normal emission, two well-resolved peaks can be distinguished. These peaks originate from the gold substrate (binding energy $E_B = 353.3$ eV), and from the palladium islands ($E_B = 340.9$ eV). The first value corresponds to bulk gold, while the second reflects the reduced state of the palladium atoms when compared with bulk material ($E_B = 340.3$ eV) and Pd^{II} (343.3 eV).[22] The small, but significant, shift of 0.6 eV to higher binding energies with respect to bulk palladium can be used as a first piece of evidence that the palladium islands are well-separated from the gold single crystal, because neither palladium on top of the gold single crystal nor palladium atoms when forming a PdAu alloy[36] on top of the gold single crystal would show any binding-energy shift with respect to

bulk palladium. On the other hand, the observed shift of 0.6 eV could be due to either final state effects,[37,38] induced by the photoemission process itself (charging of nanoscale isolated capacitors), or to bonding to the SAM.

More details about the layer sequence can be extracted from the angular dependence of the core-level spectra. The spectra show an increasing contribution of the Pd $3d_{3/2}$ core line with decreasing probing depth of the spectroscopy (i.e., increasing detection angle α). This behavior clearly reflects an enhanced attenuation of photoelectrons emitted from the gold substrate, thereby giving a second piece of spectroscopic evidence that the palladium layer is on top, rather than underneath, the SAM. In order to achieve a more quantitative picture from the spectra in Figure 3, a line-shape analysis was performed for the measured Au $4d_{3/2}$, Pd $3d_{3/2}$, and C 1s core lines by applying a numerical least-squares-fitting procedure[36] using Doniach–Sunjic lineshapes.[39] This procedure allows one to obtain reliable values for the peak intensities of the different chemical species (gold, palladium, carbon). Therefore, it allows critical comparison with models to determine if the palladium layer remains on top of, or underneath, the SAM.

The results of such a procedure are summarized in Figure 4, where the ratios of the integrated intensities of the gold substrate to either the carbon layer (left axis) or the palladium layer (right axis) are plotted for various electron-emission angles (solid symbols). The experimental intensity ratios can now be compared with predictions by using a simple layer model applying standard formulae for angle-resolved photoemission,[40,41] in which each overlayer attenuates the intensity of the photoelectron escaping from the underlying layers. Using mean-free-path values of 1.7 nm for Au $4d_{3/2}$ (Pd $3d_{3/2}$) photoelectrons,[42] and 3.4 nm for C 1s photoelectrons emitted from hydrocarbon films,[43] and taking into account a continuous organic layer on the gold substrate (0.8 nm thick, corresponding to the length of the molecules), together with palladium islands (height: one monolayer) covering only 30 % of the sample surface as found in the STM experiments, the dependence of the corresponding intensity ratios on the emission angle for the two possible layer sequences (Au/SAM/Pd or Au/Pd/SAM) can be calculated. The calculation results have been added to Figure 4 where, within experimental error, excellent agreement was found between the experimental and the calculated values for the sequence Au/SAM/Pd. This agreement is demonstrated for the intensity ratios of gold to carbon (solid line) as well as gold to palladium (dotted line). In clear contrast, the results predicted for the case where palladium atoms are underneath the organic layer (Au/Pd/SAM, dashed line) significantly deviate from the measured values. In this way, angle-resolved XPS unequivocally proves that the electrochemical approach of covering an organic SAM by palladium atoms leads to the desired layer sequence of Au/SAM/Pd.

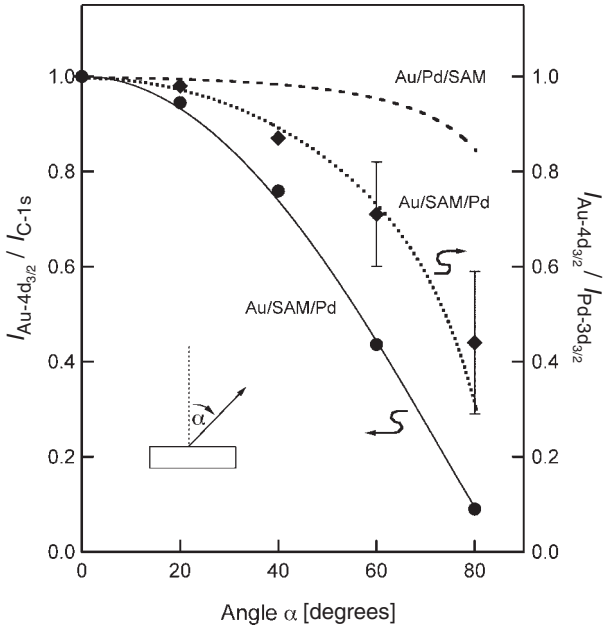

Figure 4. Ratio of the Au $4d_{3/2}$ and C 1s line intensities (left scale) as well as the Au $4d_{3/2}$ and Pd $3d_{3/2}$ line intensities (right scale) as a function of the photoelectron detection angle; experimental data as determined by a line-shape analysis of the measured core-level spectra (solid symbols); theoretical values as calculated for a SAM thickness of 0.8 nm and assuming either a layer sequence Au/SAM/Pd (solid and dotted lines) or a Au/Pd/SAM sequence (dashed line).

It is worth mentioning that the smooth variation of the measured intensity ratio for the gold and carbon signals as a function of the electron-detection angle indicates that diffraction of Au $4d_{3/2}$ photoelectrons within the single-crystal gold substrate does not significantly influence our experimental results. Otherwise, a strong modulation of this ratio with emission angle should be visible in the measured values. Using an angular resolution of $\pm 12°$ during data acquisition obviously allows such effects to be averaged out.

In conclusion, a novel technique for the electrochemical metallization of organic monolayers has been presented, based on the complexation of Pd^{II} ions with a pyridine moiety of a SAM, followed by an electrochemical reduction to Pd^0. Based on angle-resolved X-ray photoelectron spectroscopy, clear evidence was provided that the metallic layer indeed remains on top of the SAM, rather than creeping in between the SAM and the gold substrate.

Experimental

The samples were prepared in three steps: 1) the freshly annealed Au(111) electrode was immersed for 5 min (without potential control) into a 20 μM 4,4′-dithiodipyridine (Aldrich, 98 %, as received) solution prepared with ultrapure water (Sartorius, Germany, total organic carbon (toc) < 3 parts per billion, resistance 18.2 MΩ cm), which was deaerated to prevent thiol oxidation. 2) After thoroughly rinsing the thiol-modified electrode with water, the sample was incubated without potential control for 15 min in 0.1 mM $PdSO_4$ (Alfa Aesar, 99.95 %) + 0.1 M H_2SO_4 (Merck, suprapur) to allow palladium-ion adsorption on the self-assembled monolayer (SAM). 3) After rinsing again with water, the electrode was transferred to an electrochemical cell containing 0.1 M H_2SO_4. The electrode was contacted with the electrolyte at +0.7 V to prevent the unintentional reduction of the ad-

ADVANCED MATERIALS

sorbed Pd^{II}. All potentials are reported versus SCE (saturated calomel electrode), although for the scanning tunneling microscopy (STM) experiments a platinum wire was used as a pseudo-reference electrode ($E_{Pt} = +0.55 \pm 0.05$ V vs. SCE). Details about the experimental setup for cyclic voltammetry and STM are described elsewhere [26]. After their preparation, the samples for the photoemission experiments were immediately stored under an argon atmosphere, reducing the exposure time to ambient conditions during their loading into the ultrahigh-vacuum system of the electron spectrometer to less than a minute.

The photoelectron spectra were measured with a Fisons Escalab-210 system using monochromatic Al Kα radiation (1486.6 eV, spot size < 1 mm). All spectra were taken with an overall energy resolution (full width at half maximum) of 0.36 eV and an angular resolution of ±12° to avoid photoelectron-diffraction effects. To calibrate the instrument, the Fermi edge of a gold reference sample was determined, defining the origin of the binding energy scale ($E_B = 0$). It has to be emphasized that radiation damage to the SAM by the X-ray exposure could be avoided due to the small-spot X-ray source, allowing a certain sample position to be probed for times of less than 1 h, followed by moving to a new position. During that time, no measurable decreases in the corresponding core-level intensities, or changes in their line shapes, were detected.

Received: March 18, 2004
Final version: June 16, 2004

[1] K. W. Hipps, *Science* **2001**, *294*, 536.
[2] M. A. Reed, C. Zhou, C. J. Muller, T. P. Burgin, J. M. Tour, *Science* **1997**, *278*, 252.
[3] C. Kergueris, J.-P. Bourgoin, S. Palacin, C. Esteve, C. Urbina, M. Magoga, C. Joachim, *Phys. Rev. B: Condens. Matter Mater. Phys.* **1999**, *59*, 12 505.
[4] J. Chen, M. A. Reed, A. M. Rawlett, J. M. Tour, *Science* **1999**, *286*, 1550.
[5] R. P. Andres, T. Bein, M. Dorogi, S. Feng, J. I. Henderson, C. P. Kubiak, W. Mahoney, R. G. Osifchin, R. Reifenberger, *Science* **1996**, *272*, 1323.
[6] T. Ohgi, D. Fujita, *Phys. Rev. B: Condens. Matter Mater. Phys.* **2002**, *66*, 115 410.
[7] J. Zheng, Y. Zhou, X. Li, Y. Ji, T. Lu, R. Gu, *Langmuir* **2003**, *19*, 632.
[8] D. I. Gittins, D. Bethell, D. J. Schiffrin, R. J. Nichols, *Nature* **2000**, *408*, 67.
[9] D. R. Jung, A. W. Czanderna, *Crit. Rev. Solid State Mater. Sci.* **1994**, *19*, 1.
[10] E. L. Smith, A. A. Alves, J. W. Anderegg, M. D. Porter, L. M. Siperko, *Langmuir* **1992**, *8*, 2707.
[11] M. Nishizawa, T. Sunagawa, H. Yoneyama, *Langmuir* **1997**, *13*, 5215.
[12] H. Hagenström, M. A. Schneeweiß, D. M. Kolb, *Langmuir* **1999**, *15*, 7802.
[13] S. E. Gilbert, O. Cavalleri, K. Kern, *J. Phys. Chem.* **1996**, *100*, 12 123.
[14] F. P. Zamborini, J. K. Campbell, R. M. Crooks, *Langmuir* **1998**, *14*, 640.
[15] D. Oyamatsu, S. Kuwabata, H. Yoneyama, *J. Electroanal. Chem.* **1999**, *473*, 59.
[16] O. Cavalleri, A. Bittner, H. Kind, K. Kern, *Z. Phys. Chem.* **1999**, *208*, 107.
[17] L. Sun, R. M. Crooks, *J. Electrochem. Soc.* **1991**, *138*, L23.
[18] H. Hagenström, M. A. Schneeweiß, D. M. Kolb, *Electrochim. Acta* **1999**, *45*, 1141.
[19] T. Baunach, D. M. Kolb, *Anal. Bioanal. Chem.* **2002**, *373*, 743.
[20] M. A. Schneeweiß, H. Hagenström, M. J. Esplandiu, D. M. Kolb, *Appl. Phys. A: Mater. Sci. Process.* **1999**, *69*, 537.
[21] *Modern Electroplating*, 4th ed. (Eds: M. Schlesinger, M. Paunovic), Wiley, New York **2000**.
[22] H. Kind, A. M. Bittner, O. Cavalleri, K. Kern, T. Greber, *J. Phys. Chem. B* **1998**, *102*, 7582.
[23] W. J. Dressick, C. S. Dulcey, J. H. Georger, G. S. Calabrese, J. M. Calvert, *J. Electrochem. Soc.* **1994**, *141*, 210.
[24] I. Turyan, D. Mandler, *Anal. Chem.* **1997**, *69*, 894.
[25] W.-P. Zhou, T. Baunach, V. Ivanova, D. M. Kolb, *Langmuir* **2004**, *20*, 4590.
[26] T. Baunach, V. Ivanova, D. A. Scherson, D. M. Kolb, *Langmuir* **2004**, *20*, 2797.
[27] M. A. Bryant, R. M. Crooks, *Langmuir* **1993**, *9*, 385.
[28] H.-Z. Yu, N. Xia, Z.-F. Liu, *Anal. Chem.* **1999**, *71*, 1354.
[29] S. I. Ginzburg, N. N. Chalisova, *Russ. J. Inorg. Chem. (Trans. Of Zh. Neorg. Khim.)* **1968**, *13*, 648.
[30] J. A. Abys, C. A. Dullaghan, in *Modern Electroplating*, 4th ed. (Eds: M. Schlesinger, M. Paunovic), Wiley, New York **2000**, p. 483.
[31] E. Jackson, D. A. Panthony, *J. Appl. Electrochem.* **1971**, *1*, 283.
[32] R. Eskenazi, J. Raskovan, R. Levitus, *J. Inorg. Nucl. Chem.* **1966**, *28*, 521.
[33] A. M. el Aziz, L. A. Kibler, *J. Electroanal. Chem.* **2002**, *534*, 107.
[34] J. Tang, M. Petri, R. Hoyer, L. A. Kibler, D. M. Kolb, unpublished.
[35] This can safely be concluded from a measured step height which approximately corresponds to the size of a palladium atom. The observed small deviation might be due to a tip penetration into the organic layer, or to electronic effects which can also change the topographic height.
[36] G. K. Wertheim, S. B. Dicenso, *J. Electron Spectrosc. Relat. Phenom.* **1985**, *37*, 57.
[37] G. K. Wertheim, S. B. DiCenzo, S. E. Youngquist, *Phys. Rev. Lett.* **1983**, *51*, 2310.
[38] H. Hövel, B. Grimm, M. Pollmann, B. Reihl, *Phys. Rev. Lett.* **1998**, *81*, 4608.
[39] S. Doniach, M. Sunjic, *J. Phys. C: Solid State Phys.* **1970**, *3*, 385.
[40] T.-S. Lin, W. J. Partin, G. M. Damminga, T. M. Parrill, W.-J. Lee, Y.-W. Chung, *Surf. Sci.* **1987**, *183*, 113.
[41] W. F. Bergerson, J. A. Mulder, R. P. Hsung, X.-Y. Zhu, *J. Am. Chem. Soc.* **1999**, *121*, 454.
[42] *Practical Surface Analysis,* 2nd ed., (Eds: D. Briggs, M. P. Seah), Wiley, Chichester, UK **1996**, Vol. 1.
[43] P. E. Laibinis, C. D. Bain, G. M. Whitesides, *J. Phys. Chem.* **1991**, *95*, 7017.

Enhanced Field Emission of ZnO Nanowires**

By *Debasish Banerjee*, *Sung Ho Jo*, and *Zhi Feng Ren**

High-quality field emitters are very desirable for applications in a wide range of field-emission-based devices such as flat-panel displays, parallel-electron-beam microscopes, vacuum microwave amplifiers, X-ray sources, etc.[1,2] One-dimensional (1D) structures such as nanotubes and nanowires are ideal candidates for achieving high field-emission-current

[*] Prof. Z. F. Ren, D. Banerjee, Dr. S. H. Jo
Department of Physics, Boston College
Chestnut Hill, MA 02467 (USA)
E-mail: renzh@bc.edu

[**] The work performed by S. H. Jo and Z. F. Ren is supported by DOE under grant DE-FG02-00ER45805, and the work done by D. Banerjee is supported by the US Army Natick Soldier Systems Center under grant DAAD16-03-C-0052.

  DOI: 10.1002/adma.200400629